Journal of Geochemical Exploration 197 (2019) 143–158

Contents lists available at ScienceDirect

Journal of Geochemical Exploration

journal homepage: www.elsevier.com/locate/gexplo

Integrating sequential indicator simulation and singularity analysis to analyze uncertainty of geochemical anomaly for exploration targeting of tungsten polymetallic mineralization, Nanling belt, South China

Yue Liu[a,b,c,*], Qinglin Xia[d,e], Emmanuel John M. Carranza[f]

[a] State Key Laboratory of Desert and Oasis Ecology, Xinjiang Institute of Ecology and Geography, Chinese Academy of Sciences, Urumqi, Xinjiang 830011, China
[b] Xinjiang Research Centre for Mineral Resources, Xinjiang Institute of Ecology and Geography, Chinese Academy of Sciences, Urumqi, Xinjiang 830011, China
[c] Xinjiang Key Laboratory of Mineral Resources and Digital Geology, Urumqi, Xinjiang 830011, China
[d] Cooperative Innovation Center for Scarce Mineral Resources Exploration, China University of Geosciences (Wuhan), Wuhan, Hubei 430074, China
[e] Faculty of Earth Resources, China University of Geosciences, Wuhan 430074, China
[f] Geological Sciences, School of Agriculture, Engineering and Sciences, University of KwaZulu-Natal, Westville, South Africa

ARTICLE INFO

Keywords:
Sequential indicator simulation
Singularity analysis
Geochemical anomaly separation
Uncertainty assessment
Nanling belt

ABSTRACT

The Nanling belt (South China) is one of the most important metallogenic region in the world in regard to tungsten polymetallic resources. In this belt and surrounding area, the most important elements accompanying tungsten deposits are Sn, Bi, and Mo. Modelling the spatial variability and uncertainty of W, Sn, Bi, and Mo anomalies is critical for tungsten polymetallic exploration risk assessment. However, traditional interpolation methods (e.g., kriging, polynomial trend surface and inverse distance weighted method) for modelling continuous geochemical fields based on sparse sampling data provide smoothed representations of element concentrations, which often result in unreliable decisions. Here, uncertainty analysis of geochemical anomaly for tungsten polymetallic exploration targeting was investigated through combined sequential indicator simulation and local singularity analysis. Anomalous thresholds of E-type singularity indices for the selected elements (W, Sn, Mo and Bi) were determined by singularity-quantile plot analysis. The distribution pattern of probability of not exceeding a threshold singularity index was obtained from a series of equally probable representations of singularity indices of individual elements (W, Sn, Mo and Bi) based on local and spatial uncertainty algorithms. Based on the four probabilistic models, one per element, a synthetic probability map was produced for uncertainty assessment of geochemical anomaly for exploration targeting. The results indicate that zones with very high probabilities are significantly correlated with known tungsten polymetallic deposits and are closely associated with lithostratigraphic contacts. These results provide for important decision-making for risk evaluation of tungsten polymetallic exploration targeting based on spare stream sediment geochemical data in the Nanling belt.

1. Introduction

In the initial stages of mineral resources investigations, surface geochemical sampling data (e.g., from sediments, soils, water) are commonly employed to distinguish geochemical anomaly from background (Zhao et al., 2012; Yuan et al., 2015; Carranza, 2017a, 2017b; Agterberg, 2014; Chen and Wu, 2017; Chen and Cheng, 2016; Zhang et al., 2016; Liu et al., 2013, 2014a, 2016, 2017; Yousefi, 2017; Tan et al., 2018; Zuo, 2017; Wang et al., 2017; Parsa et al., 2017; Cracknell and de Caritat, 2017; Xiao et al., 2018). However, limited or sparse surface geochemical samples can lead to a certain degree of uncertainty (e.g., bias and inconsistent spatial estimation) in spatial prediction results when traditional interpolated methods (e.g., kriging and inverse distance weighting) are applied to model continuous geochemical fields from such sparse point geochemical data. Although spatial prediction accuracy can be efficiently improved by means of increasing sampling density (Goovaerts, 2001), it generally takes significant amounts of time and money to conduct geochemical sampling surveys with high sampling density. Therefore, mapping of geochemical anomaly for identifying potential mineralized areas inevitably involves spatial uncertainties, which propagate into subsequent geochemical field modelling and fundamentally impact the ultimate results and the decision-

* Corresponding author.
E-mail address: liuyue@ms.xjb.ac.cn (Y. Liu).

https://doi.org/10.1016/j.gexplo.2018.11.012
Received 20 July 2018; Received in revised form 16 October 2018; Accepted 26 November 2018
Available online 29 November 2018

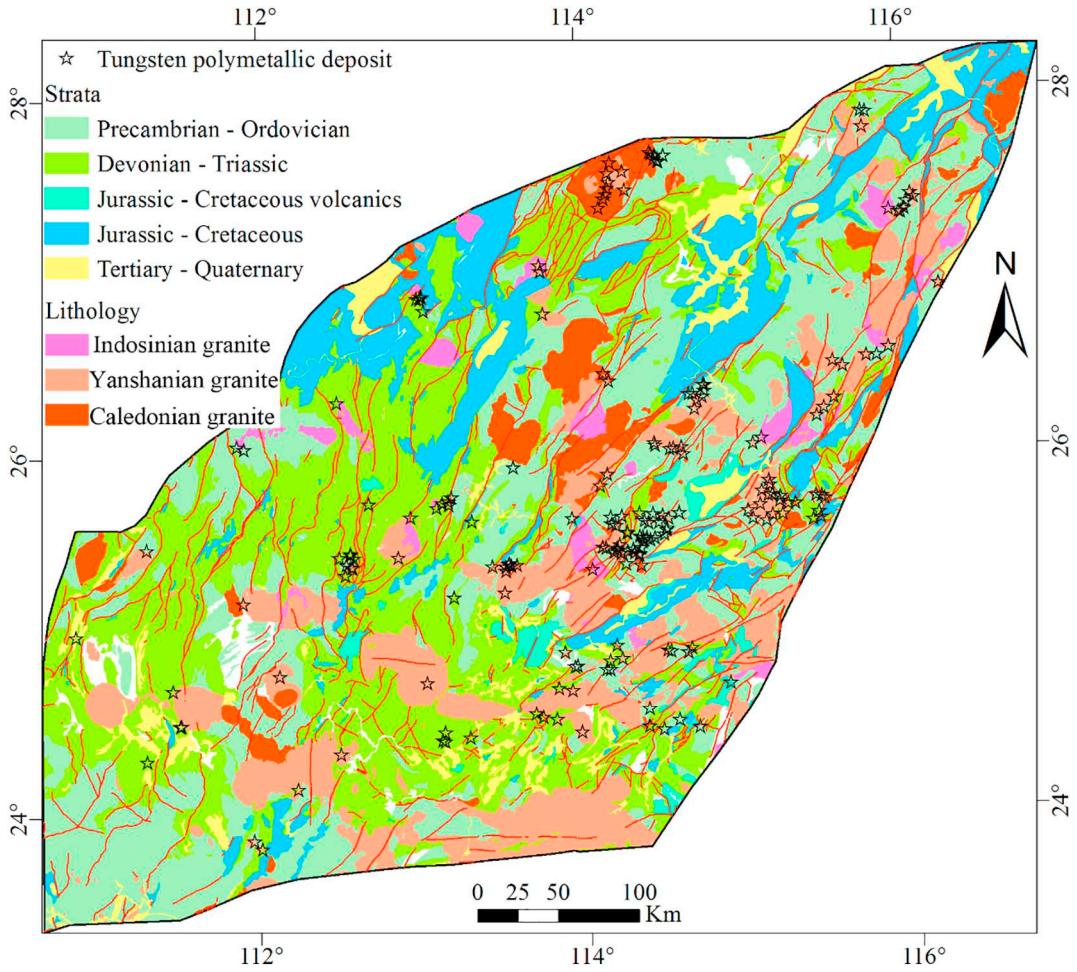

Fig. 1. Simplified geological map of the Nanling belt, South China.

making analysis (Goovaerts, 1997; Zhao et al., 2005; Liu et al., 2018a). Practically, spatial uncertainties in estimates from sparse data can be addressed with reasonable methods; for example, a method of weighted drainage catchment basin (WDCB), which is independent of sampling sites and density, and thus avoids the influence of data interpolation, has been developed to map stream sediment geochemical anomalies (Yousefi et al., 2013). Theoretically, the application of geostatistical simulation techniques provides for modelling spatial uncertainty of estimates at unsampled locations.

Geostatistical simulation algorithms are increasingly being used for uncertainty modelling mainly because traditional interpolation methods only produce a unique result – the so-called interpolated map – in which local details (e.g., extreme values) in spatial variability of the target attribute being mapped are commonly smoothed out. In contrast, geostatistical simulation results in a more realistic model of the spatial variation of the target attribute and provides a basis for analysis of spatial uncertainty associated with spatial predictions (Goovaerts, 1997; Deutsch and Journel, 1998). Several equiprobable realizations of element concentrations characterized by similar spatial distribution patterns can be obtained by means of geostatistical simulation techniques, and spatial variations among such realizations provide a measure of spatial uncertainty (Goovaerts, 2001; Deutsch and Journel, 1998; Emery and Ortiz, 2012). In recent years, geostatistical simulation techniques have been widely applied for quantification of uncertainties in geochemical systems (Afzal et al., 2015; Sadeghi et al., 2015; Mery et al., 2017; Paithankar and Chatterjee, 2018; Hosseini and Asghari, 2018; Rahimi et al., 2018; Qu and Deutsch, 2018). For geochemical anomaly uncertainty analysis, a method by integrating sequential Gaussian simulation (SGS) with singularity analysis has been proposed

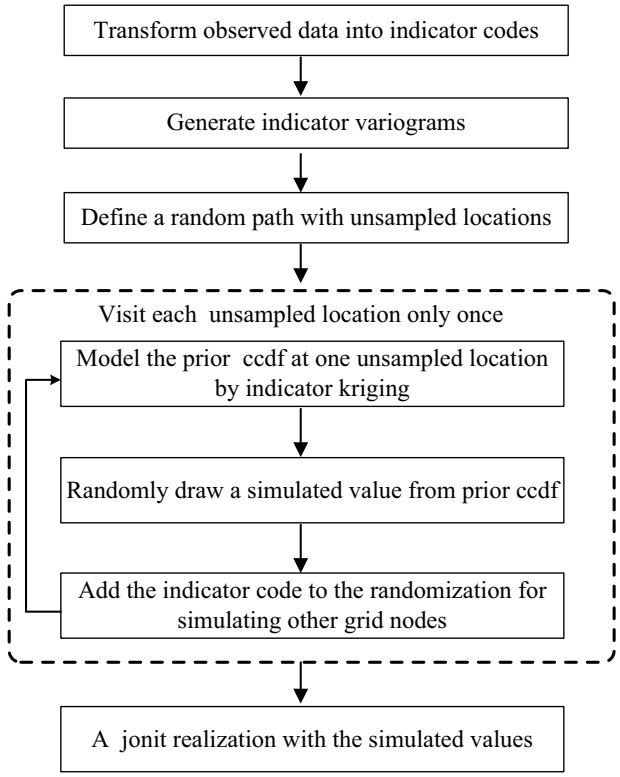

Fig. 2. Flow chart illustrating the procedure of sequential indicator simulation.

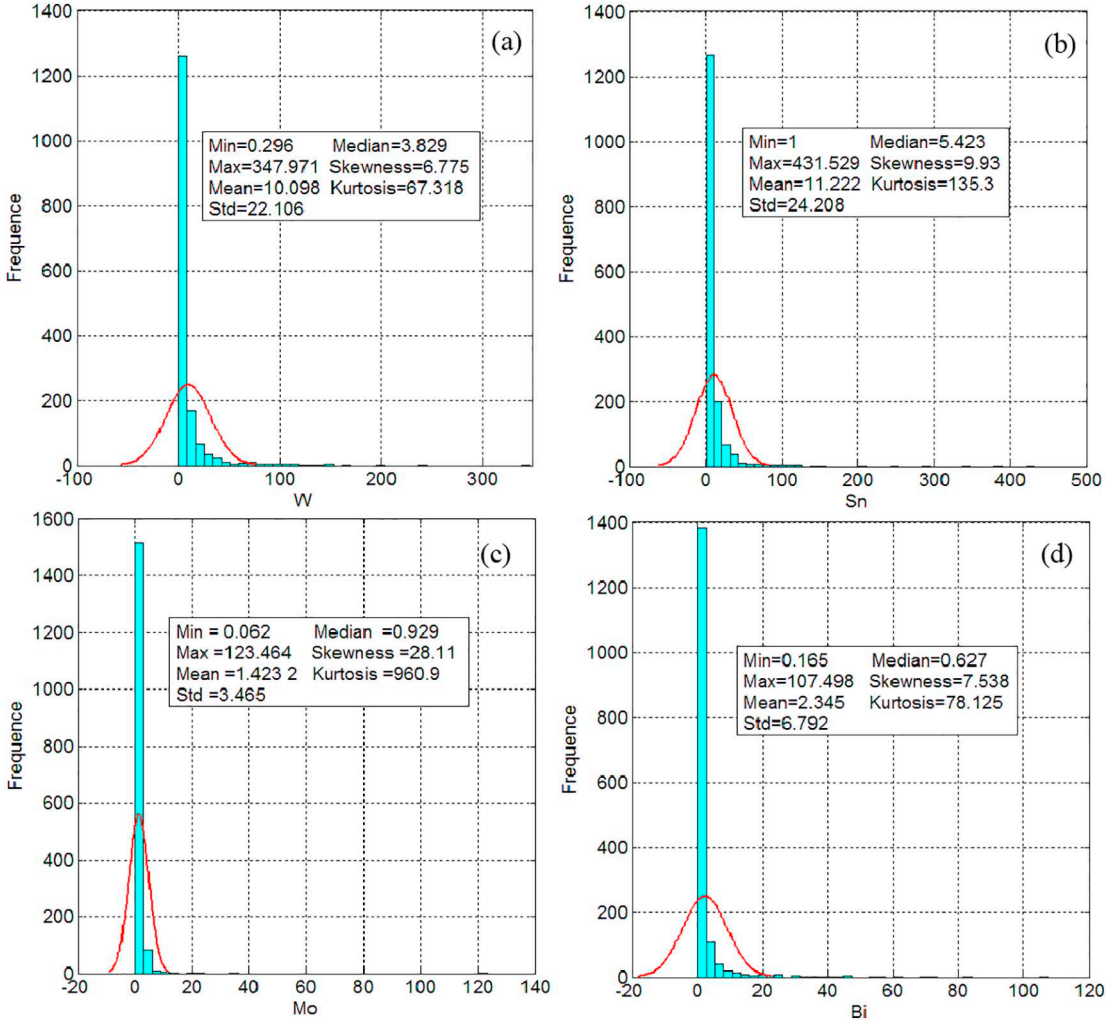

Fig. 3. Histograms with relevant statistical parameters of (a) W, (b) Sn, (c) Mo, and (d) Bi.

Table 1
Experimental indicator variogram models of four elements based on quantile thresholds.

Threshold	Cutoff value (ppm)	C_0	C	$C_0 + C$	$C_0/(C_0 + C)$	R^2	RSS	Range (m)
20% (W)	2.413	0.062	0.079	0.141	43.97%	0.951	3.20E-03	71,600
40% (W)	3.080	0.096	0.130	0.226	42.48%	0.975	3.90E-04	78,900
60% (W)	4.177	0.093	0.146	0.239	38.91%	0.977	3.50E-04	84,300
80% (W)	7.807	0.074	0.095	0.169	43.79%	0.964	2.40E-04	65,600
20% (Sn)	3.490	0.068	0.089	0.157	43.31%	0.984	1.40E-04	60,300
40% (Sn)	4.493	0.078	0.155	0.233	33.48%	0.980	3.10E-04	71,600
60% (Sn)	6.328	0.076	0.160	0.236	32.20%	0.963	9.30E-04	67,900
80% (Sn)	10.817	0.059	0.115	0.174	33.91%	0.961	4.10E-04	69,300
20% (Mo)	0.621	0.074	0.078	0.152	48.68%	0.874	1.70E-04	67,200
40% (Mo)	0.818	0.097	0.114	0.211	45.97%	0.894	1.10E-03	86,500
60% (Mo)	1.104	0.095	0.123	0.218	43.58%	0.834	1.30E-03	94,000
80% (Mo)	1.630	0.065	0.098	0.163	39.88%	0.994	8.00E-05	75,400
20% (Bi)	0.395	0.062	0.076	0.138	44.93%	0.972	9.00E-05	61,800
40% (Bi)	0.501	0.083	0.143	0.226	36.73%	0.989	1.50E-04	71,700
60% (Bi)	0.693	0.082	0.160	0.242	33.88%	0.945	1.30E-03	76,300
80% (Bi)	1.811	0.064	0.109	0.173	36.99%	0.852	7.60E-04	69,400

Note: C_0: nugget variance; C: Sill variance; $C_0 + C$: total variance; $C_0/(C_0 + C)$: coefficient of variation; R^2: squared correlation coefficient; RSS: residual sum of squares; Range: lag distance.

to model gold anomaly uncertainty in the west Tianshan region, China (Liu et al., 2018a).

The goals of this study are (a) to integrate sequential indicator simulation (SIS) and local singularity analysis for geochemical anomaly uncertainty analysis, (b) to quantify spatial uncertainty of estimated element concentrations (W, Sn, Mo and Bi) related to tungsten polymetallic mineralization, (c) map the probability of geochemical anomaly occurrence related to tungsten polymetallic mineralization

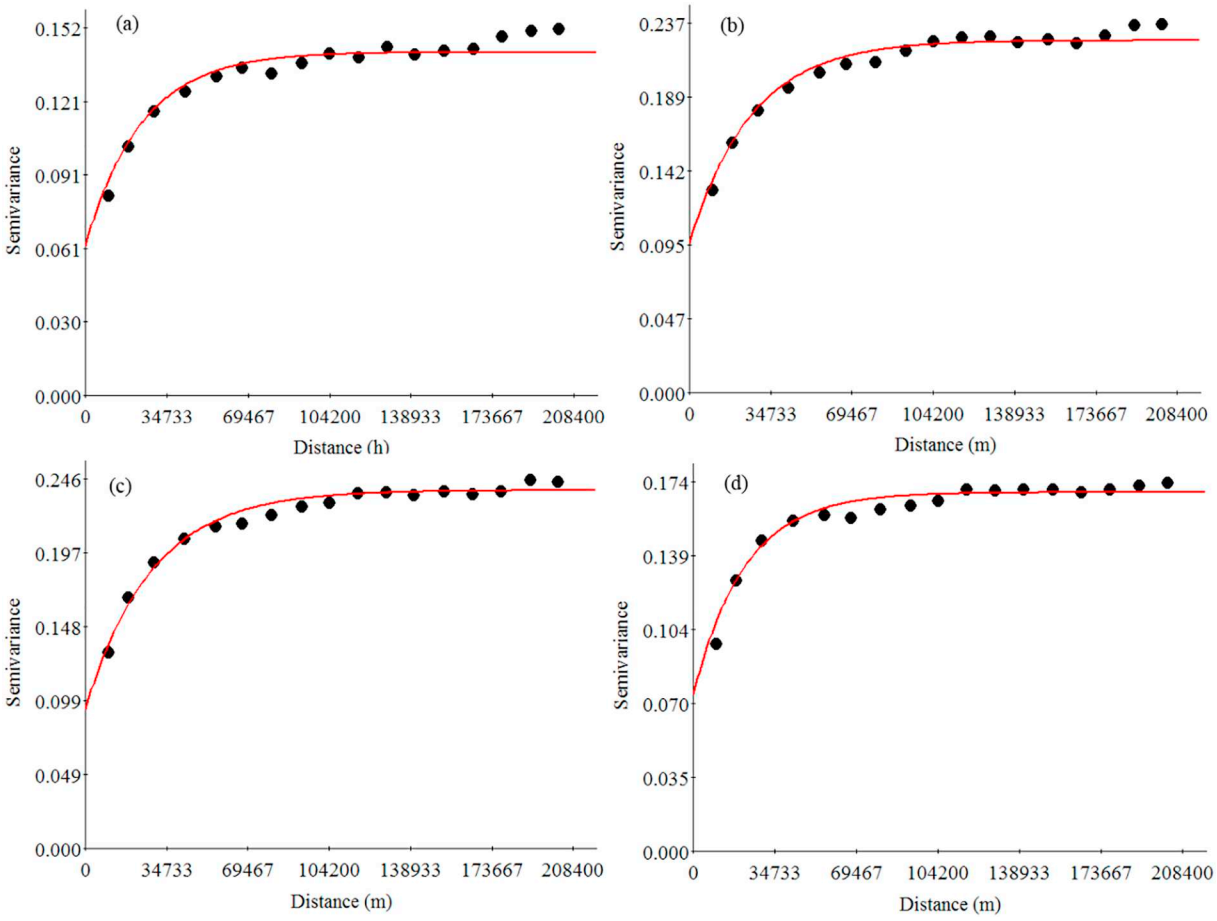

Fig. 4. Experimental (black points) and fitted (red lines) indicator semivariograms for the (a) 20th, (b) 40th, (b) 60th, and (c) 80th percentiles of W data. (For interpretation of the references to colour in this figure legend, the reader is referred to the web version of this article.)

based on the critical thresholds determined by singularity-quantile poly analysis, and (d) assess risks associated with exploration targeting for tungsten polymetallic deposits posed by geochemical anomalies of four individual elements, namely W, Sn, Mo and Bi. These research goals pertain to the study area - the Nanling metallogenic belt - but the results/findings can be applied to similar geological and geomorphological settings.

2. Geological background

The Nanling belt is the most important part of the South China granitic province because of its tectonic and metallogenic significance. The strata exposed in the study area are mainly composed of intensely folded Late Proterozoic basement and Late Paleozoic-Mesozoic sedimentary cover (Fig. 1) (Xu et al., 2005; Peng et al., 2006; Mao et al., 2007). The basement mainly consists of Neoproterozoic metamorphic argillaceous sandstones interbedded with volcanic rocks, metamorphic sedimentary flysch, pyroclastic rocks and siliceous rocks. The sedimentary cover is mainly composed of Late Devonian to Early Triassic sandstone, mudstone and carbonate rocks, developing littoral facies, neritic facies, and interactive marine and terrestrial deposits with total thickness of about 7000–8000 m (Mao et al., 2007). The Triassic-Paleogene lithological units consist of discontinuous sedimentary sequences characterized by volcanoclastic rocks, detrital rocks and red beds that were formed in rifted-basins (Shu et al., 2006; Mao et al., 2007; Wang et al., 2012).

Since the Early Paleozoic, the Nanling belt has experienced extensive magmatic activities and multi-phased orogenies that mainly occurred in three periods, namely Cambrian-Silurian, Late Permian-Triassic and Jurassic (Chen et al., 1989; Mao et al., 2007), which resulted in abundant granite intrusions, which intruded into the Proterozoic and Paleozoic sedimentary rocks (Zhou et al., 2006; Mao et al., 2007; Hu and Zhou, 2012; Chen et al., 2013) and covering a total area of roughly 41 $\times$ 10^3 km^2 (Fig. 1). The basement and sedimentary cover of the belt have undergone intense intra-continental deformation due to the effect of the Indosinian orogeny, which resulted in the extensive magmatic activities and the emplacement of numerous Indosinian granites (Shu et al., 2006; Zhou et al., 2006). The regional structural regime in the Nanling belt changed from compressional to extensional tectonism, which led to the generation of numerous granite intrusions during the Yanshanian orogeny (Zhou, 2003; Mao et al., 2007; Hua et al., 2005). Spatially, lattice faults with different trends, namely *E*-W, N-S, NW and NE, controlled the emplacement of granites.

The complex geological processes associated with the magmatic activities resulted in the formation of various types of tungsten polymetallic mineralization including quartz-vein-, skarn-, altered granite-, and greisen-types (Hu and Zhou, 2012; Zhao et al., 2017). Studies indicate that the Caledonian granites mainly belong to peraluminous S-type and parts of them are related to the formation of tungsten polymetallic deposits (Zhang et al., 2011); the Indosinian granites were formed in a post-collision extensional tectonic environment, showing weak relationship with tungsten polymetallic deposits in space (Fig. 1; Sun et al., 2003); and the Yanshanian was the most important epoch for magmatism and metallogenesis in the south China, when a large number of tungsten polymetallic deposits were formed such as the Shizhuyuan, Xintianling, Dajishan, Xihuashan, Piaotang, and Xianghualing deposits (Zhou et al., 2006; Xu and Zhu, 1988; Liu et al., 2014b; Chen et al., 2015; Zhao et al., 2017). Ore-forming ages of the

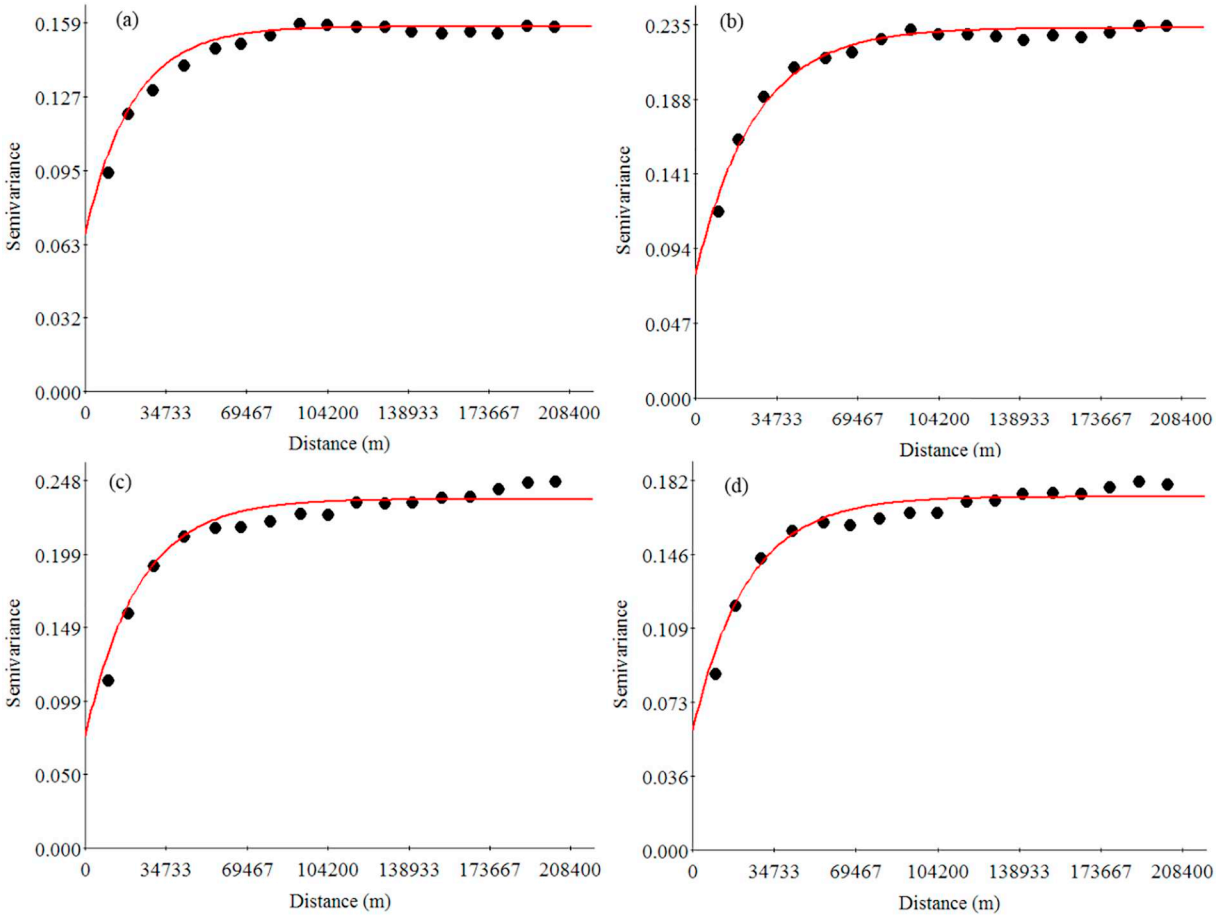

Fig. 5. Experimental (black points) and fitted (red lines) indicator semivariograms for the (a) 20th, (b) 40th, (b) 60th, and (c) 80th percentiles of Sn data. (For interpretation of the references to colour in this figure legend, the reader is referred to the web version of this article.)

majority of large-size deposits range mainly from the Middle Jurassic to the Early Cretaceous, whereas Triassic tungsten polymetallic deposits are relatively small and sparse (Chen et al., 2008, 2013; Mao et al., 2013; Hu and Zhou, 2012). It has been found that anomalous W-Sn accumulations that have taken place in the South China continent are closely associated with the metallogenic system of Mesozoic granite province (Wang et al., 2013). Alkalic feldspar granite, slate, phyllite and schist are usually characterized by high background contents of tungsten and tin, and are generally considered as the sources of the main ore-forming materials for the tungsten polymetallic deposits (Li, 1991; Chi et al., 2012; Wei et al., 2006).

Mineralization in the Nanling belt, being one of the most important metallogenic belts in the world, is attributed to large-scale tungsten polymetallic metallogenesis during the Mesozoic period that resulted in the formation of abundant tungsten and tin resources, which are estimated to be 1.7 and 1.2 million tons, respectively (Zhao et al., 2017). Previous studies indicate that tungsten deposits in South China are usually accompanied with Ag, Sb, Sn, Mo, Cu, Bi, Hg and rare earth element (Hu and Zhou, 2012; Mao et al., 2013; Li et al., 2017; Hu et al., 2017; Zhao et al., 2017), in which Sn, Bi and Mo are most commonly accompanying elements (Hua et al., 2008).

3. Methods and data

3.1. Sequential indicator simulation

The SIS considers the spatial variation of observed data at sampled locations and the spatial variation of estimates at unsampled locations (Deutsch and Journel, 1998; de Souza and Costa, 2013). The advantages of SIS over Gaussian simulation techniques are that it provides greater flexibility in accounting for different variation models at different thresholds by using binary data and that it does not require data to satisfy normal/lognormal distribution. In SIS, indicator kriging is applied to determine the prior conditional cumulative distribution function (CCDF) at each unsampled location by coding each observed concentration value into K indicator values. For geochemical data, SIS generates a set of equiprobable concentration realizations of an element and use the variations in concentration realizations as a measure of uncertainty.

Following Deutsch and Journel (1998), Deutsch (2006), Goovaerts (2001) and Emery (2004), a general flow chart for SIS procedure includes several sequential steps, summarized in Fig. 2, which implement just the first realization. Therefore, the sequential steps are repeated with different random paths by passing through all nodes to produce the remaining realizations.

3.2. Singularity analysis

Singularity theory describes extreme geo-processes that result in significant amounts of energy release or material accumulation to occur within a narrow space-time interval (Cheng, 2007; Cheng and Agterberg, 2018). In exploration geochemistry, singularity analysis allows for characterization of the fractal/multifractal properties of element concentration distribution in the Earth's crust. The singularity index, α, is commonly calculated by a window-based method in 2-dimensional space. The average spatial density of metal concentrations, $\rho[A(\varepsilon)]$ can be obtained based on the following power-law relationship:

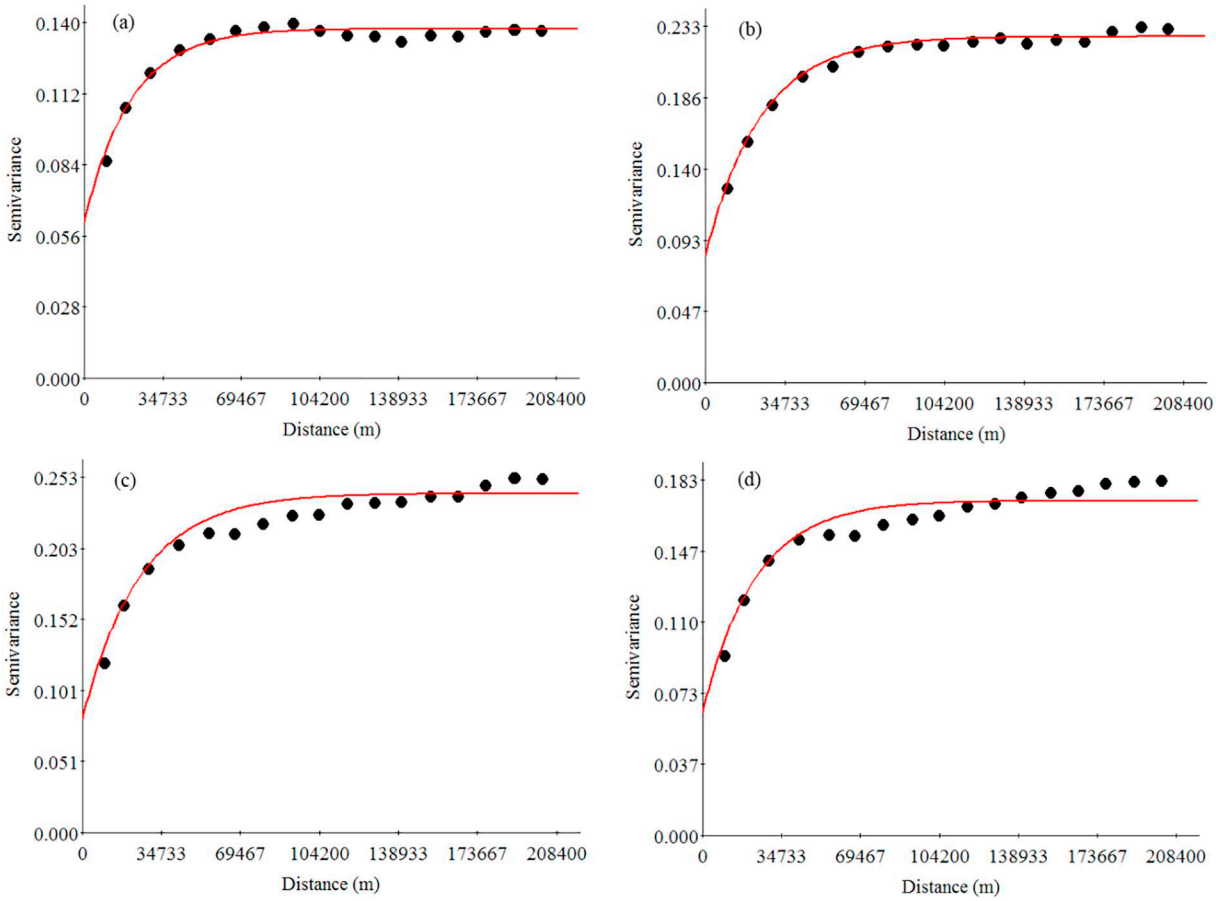

Fig. 6. Experimental (black points) and fitted (red lines) indicator semivariograms for the (a) 20th, (b) 40th, (b) 60th, and (c) 80th percentiles of Mo data. (For interpretation of the references to colour in this figure legend, the reader is referred to the web version of this article.)

$$\rho[A(\varepsilon)] = \frac{\mu[A(\varepsilon)]}{\varepsilon^2} = c \cdot \varepsilon^{\alpha-2} \tag{1}$$

where A is the study area, ε is window size, c is the fractal density (Cheng, 2016; Chen and Cheng, 2017; Liu et al., 2018a). On a log-log plot of $\rho[A(\varepsilon)]$ versus ε, the slope (α-2) can be estimated by least squares method. From a statistical point of view, values of $\alpha \approx 2$ obey a normal or lognormal distribution whereas values of $\alpha \neq 2$ may follow fractal/multifractal distributions (Cheng, 2007; Cheng and Agterberg, 2009). In the application of singularity analysis to geochemical anomaly identification, positive singularity indices of $\alpha < 2$ are interpreted to correspond to element enrichment, whereas negative singularity indices of $\alpha > 2$ are interpreted to correspond to element depletion (Cheng, 2007). Recently, a singularity-quantile (S-Q) method, developed by Liu et al. (2017, 2018b) based on singularity analysis and quantile-quantile plot analysis, can be employed to partition hybrid geochemical populations in frequency domain through the plot of standard normal quantiles versus singularity index quantiles. The S-Q method is efficient in determining critical thresholds of singularity indices and allows for classification of geochemical patterns into three groups, namely element depletion, element average and element enrichment. Detailed introduction to the S-Q method is described below in Section 4.5.

3.3. Uncertainty assessment

3.3.1. Local uncertainty analysis

The local uncertainty of an estimate at location x can be expressed as the probability that an unknown value $z(x)$ at location x is smaller (or greater) than a given threshold. In this study, we focus on assessing uncertainty of tungsten polymetallic geochemical anomaly derived by local singularity analysis. According to the concept of singularity analysis described above, the local uncertainty of a α-value can be expressed by quantifying the geochemical anomaly probability that its α-value does not exceed a threshold of low singularity index (i.e., $\alpha_c < 2$). The local uncertainty can be defined as (Goovaerts, 2001):

$$\text{Prob}_{SIS}[\alpha(x_i) < \alpha_c] = \frac{n(x_i)}{L} \quad i = 1, 2, \cdots, N \tag{2}$$

where α_c is the threshold of low singularity index and it is < 2, $n(x)$ is the number of singularity index realizations (SIRs) that are smaller than α_c at location x_i, and L is the total number of simulated SIRs. It should be noted that the SIRs can be calculated by a complied SIRs batch algorithm designed in Matlab R2013 software, in which the SIRs batch algorithm is performed on a series of equally probable realizations of element concentrations to generate a series of corresponding SIRs.

3.3.2. Spatial uncertainty analysis

Spatial uncertainty is expressed by the joint uncertainty of estimates across the whole study area (Goovaerts, 2001; Qu et al., 2015; Liu et al., 2018a). For singularity indices at location x_i, suppose that there are N locations, x_1, x_2, …, x_N across the area A; the probability of all singularity indices at the N locations being smaller than the low threshold singularity index is expressed by the joint probability of L SIRs across each node, thus:

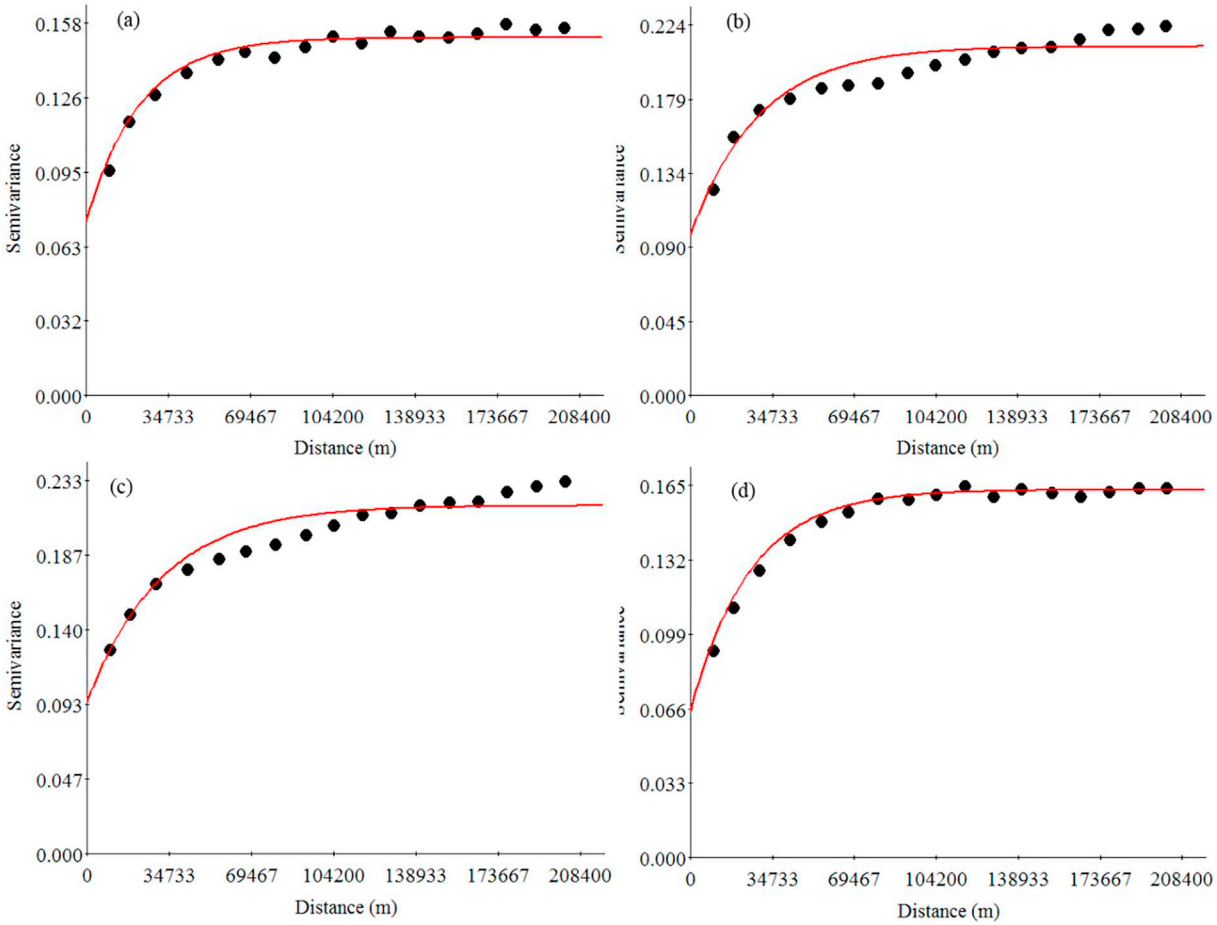

Fig. 7. Experimental (black points) and fitted (red lines) indicator semivariograms for the (a) 20th, (b) 40th, (b) 60th, and (c) 80th percentiles of Bi data. (For interpretation of the references to colour in this figure legend, the reader is referred to the web version of this article.)

$$\mathrm{Prob}_{SIS}[\alpha(x_1) < \alpha_c, \alpha(x_2) < \alpha_c, \cdots, \alpha(x_N) < \alpha_c] = \frac{n(x_1, x_2, \cdots, x_N)}{L} \quad i = 1, 2, \cdots, N \tag{3}$$

where α_c is the threshold of low singularity index and it is < 2, L is the number of simulation SIRs, N is the number of grid nodes, and $n(x_1, x_2, \ldots, x_N)$ is the number of SIRs that have all simulation values at location x_i being smaller than a low threshold (α_c) in the L SIRs.

3.4. Data

Regional geochemical surveys at a scale of 1:200,000 have been carried out since 1979 as part of the Chinese National Geochemical Mapping Project (CNGMP), which has covered > 7 million square kilometers in China including the Nanling belt (South China) (Xie et al., 1997). This study pertains to part of the Nanling belt, which is covered by 1617 stream sediment samples that are evenly distributed across the study area, and the sampling density is about one sample per 144 km^2. The samples have been analyzed for 39 elements (Bi, Cu, P, La, Li, Ag, Sn, Au, Mo, Th, U, W, Sb, Hg, Mn, Cr, Sr, Nb, Pb, Ni, Ti, Y, Cd, Co, Ba, Be, V, Zn, B, As, Zr, F, Fe_2O_3, K_2O, CaO, MgO, Na_2O, Al_2O_3 and SiO_2), including trace, minor and major elements by means of multi-instrument and multi-method approaches, namely inductively coupled plasma-atomic emission spectrometry (ICP-AES), X-ray fluorescence (XRF), and inductively coupled plasma-mass spectrometry (ICP-MS) in combination with other methods (Wang et al., 2007; Xie et al., 1997; Liu et al., 2016, 2018c). For this study, only data for W, Sn, Mo and Bi were used for geochemical anomaly uncertainty analysis because they are closely associated with tungsten polymetallic mineralization (Hua et al., 2008; Mao et al., 2013; Hu and Zhou, 2012; Hu et al., 2017; Li et al., 2017).

4. Results and discussion

The simulation results (e.g., realizations and SIRs) were calculated using software version 2.1 of SGeMS (Remy et al., 2009). The SIRs batch algorithm was designed in Matlab R2013 software to perform on a set of realizations of element concentrations so as to obtain a set of corresponding geochemical anomaly maps (realizations). Map visualization and representation in space were processed using ArcGIS 10.3 software. The singularity analysis and SIS method were performed on ASCII data that were transformed from rasterized image with grid size of 2 km × 2 km.

4.1. Preliminary data statistics

Histograms and statistical parameters such as maximum (Max), minimum (Min), standard deviation, skewness and kurtosis provide a powerful tool for rapid examination of geochemical distribution patterns, among which kurtosis and skewness are important indicators for estimating whether or not data follow normal distribution (Liu et al., 2018b). Fig. 3 shows histograms of W, Sn, Mo and Bi data with related statistical parameters. The skewness and kurtosis indicate that concentrations of W, Sn, Mo and Bi deviate from normal distribution

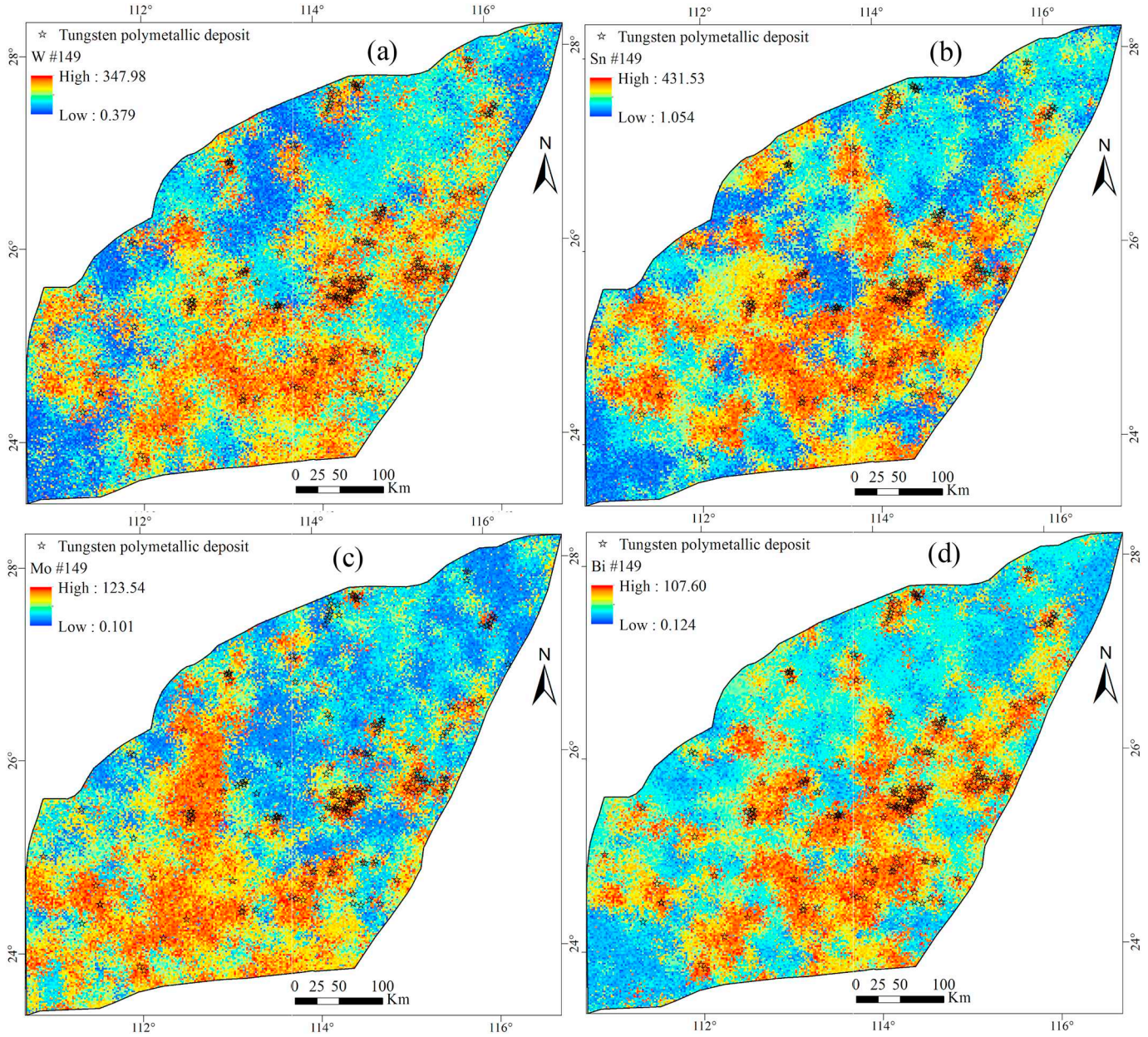

Fig. 8. Maps of simulated concentrations for realization #149: (a) W, (b) Sn, (c) Mo and (d) Bi.

significantly, especially the Mo distribution. As a result, the SIS technique was adapted to model element distribution patterns since these data do not meet the requirement of multi-Gaussian assumption.

4.2. Indicator variogram analysis

The concentrations of each element were transformed into indicator codes by means of indicator kriging method. The indicator codes are usually defined by 1 and 0. The cutoff values of concentrations per element were set to be four percentiles, namely 20%, 40%, 60%, and 80% (Table 1). Then, the indicator variograms of W, Sn, Mo and Bi were obtained based on variogram analysis (Figs. 4, 5, 6, 7). The well-fitted exponential indicator variogram models were determined using coefficient of variation (R^2) and residual sum of squares (*RSS*). Here, only four cutoff values of element concentrations were used to build the prior CCDF because extreme threshold values used in indicator variogram analysis are not well defined when too many cutoff values are used (Goovaerts, 1997; Juang et al., 2004). Figs. 4, 5, 6, 7 and Table 1 show that the indicator variograms and fitted variogram models have clear differences and spatial structures, indicating that application of the four cutoffs for indicator variogram analysis is sufficient to characterize the global spatial variability characteristics.

The coefficient of variation (*CV*), expressed as $C_0/(C_0 + C)$, was used to measure spatial heterogeneity (Cambardella et al., 1994), where C_0 is nugget variance and C is still variance. The strong spatial dependence of a target attribute across the study area is indicated by *CV* values close to 0, while a *CV* value close to 1 shows weak spatial dependence or randomness in terms of spatial heterogeneity of a target attribute. According to Cambardella et al. (1994), *CV* values larger than 75% shows weak spatial dependence, *CV* values between 25% and 75% show moderate spatial dependence, and *CV* values less than25% show strong spatial dependence. From Table 1 and Figs. 4, 5, 6, 7, the $C_0/(C_0 + C)$ ratios of the indicator variogram models for each of the four indicator variables (W, Sn, Mo and Bi) range from 32.2% to 48.68%,

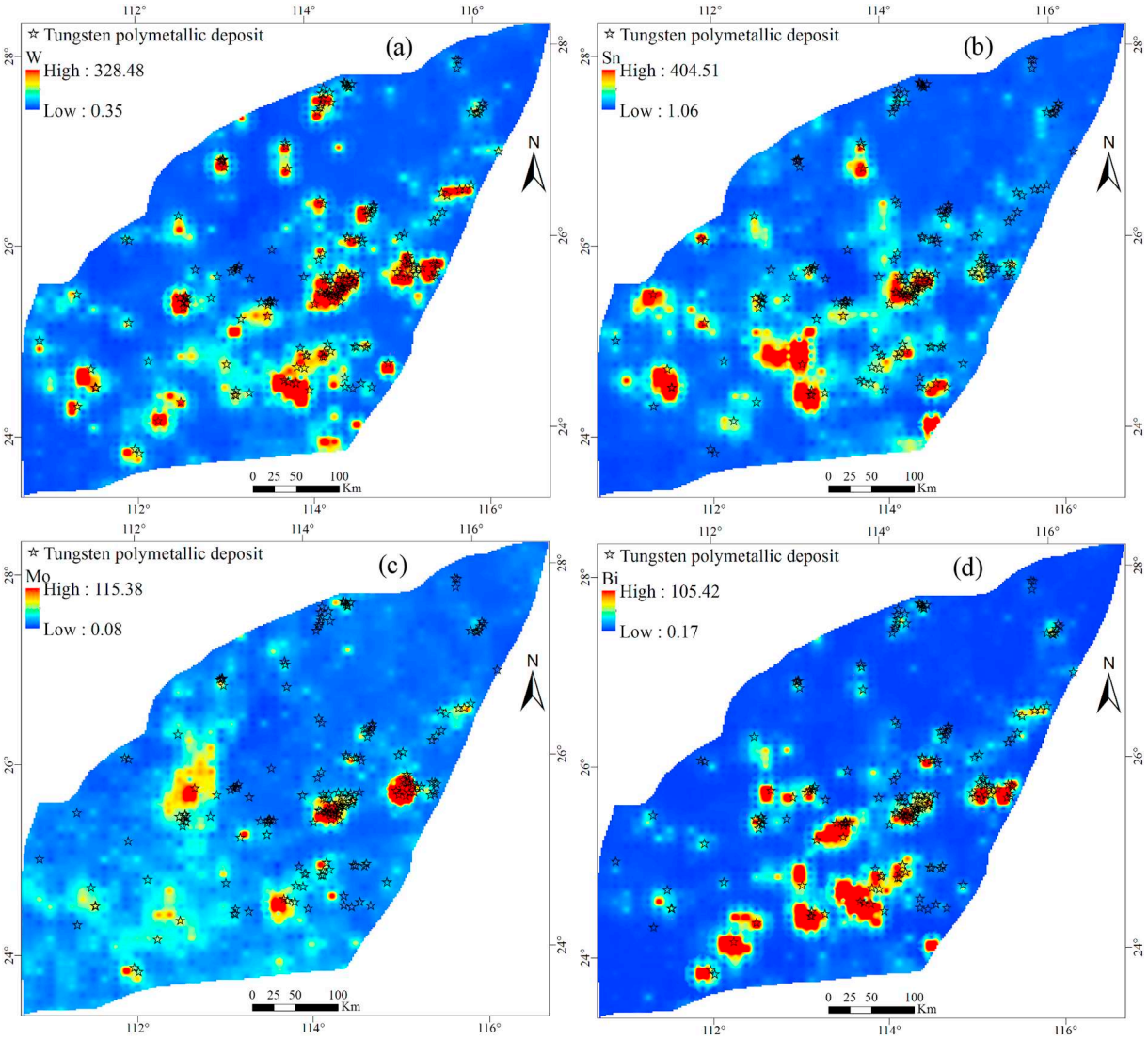

Fig. 9. IDW interpolation maps for: (a) W, (b) Sn, (c) Mo and (d) Bi.

exhibiting moderate spatial dependence. According to Cambardella et al. (1994), moderate spatial dependence may be caused by intrinsic geologic factors (e.g., sediments properties, weathering of parent rocks) and extrinsic anthropogenic factors (e.g., mining, urban development and land use).

4.3. Spatial distribution of mineralization-related element concentrations

Two hundred equiprobable concentration realizations of the individual elements (W, Sn, Mo and Bi) were generated by SIS based on simple kriging and indicator variogram models, and each of them represents a probable realistic spatial distribution of concentrations per element. The 200 concentration realizations are visually similar not only in terms of element concentration values but also in terms of their spatial distribution patterns, because they honor original conditional data and reproduce the key statistical characteristics of target element distribution, such as global spatial correlation and histogram (Goovaerts, 2001). Randomly selected realizations depicted by #149 for each of the four elements (W, Sn, Mo and Bi) are shown in Fig. 8. The maximum and minimum concentrations of individual elements are approximately equal to their original measured values as shown in Fig. 3, implying that these equiprobable concentration realizations do not change the data structures under the constraint of CCDF. However, the maps interpolated by inverse distance weighting (IDW) (Fig. 9) show that the maximum values for W, Sn, Mo and Bi are 328.48, 404.51, 115.38 and 105.42, respectively, less than the measured maximum values (Fig. 8) because of smoothing effect. More importantly, IDW interpolation is a deterministic method while geostatistical simulation techniques allow for quantification of spatial uncertainty of a target attribute.

The maps show that W, Sn and Bi have more similar spatial distribution trends compared to the spatial distribution of Mo (Fig. 8). Zones with high concentrations of W, Sn and Bi are mainly present in the southern and central parts of the Nanling belt, while zones with high concentrations of Mo mostly appear in the western parts of the study area. As demonstrated in Liu et al. (2014b, 2018d), the multi-element association of W-Sn-Mo-Bi-Ag-Cd-Be represents important controls because it indicates that basement rocks provided sources of major ore-forming materials for the formation of tungsten polymetallic deposits. Thus, the results here indicate that the zones with high concentrations of W, Sn and Bi (Fig. 8a, b and d) are mainly located in both Mesozoic granites and Devonian-Triassic sedimentary cover, which have been proven to be endowed with high geochemical background of W (Hu and Zhou, 2012; Hu et al., 2017; Li et al., 2017; Mao et al.,

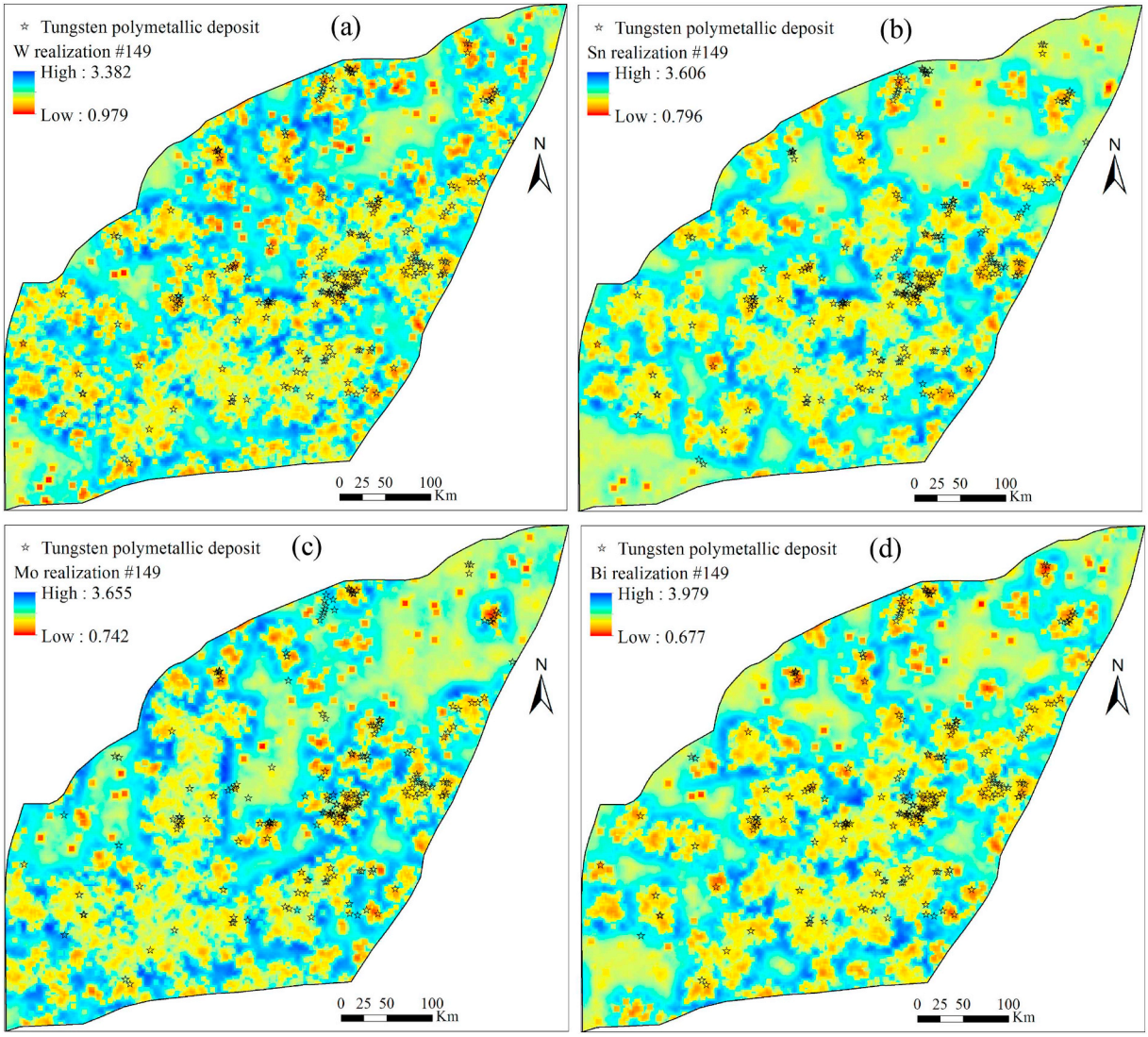

Fig. 10. Maps of simulated SIRs for #149: (a) W, (b) Sn, (c) Mo and (d) Bi.

2013). Fig. 8c shows that the zones with high Mo concentrations are mainly distributed in the western parts of the study area where Devonian-Triassic strata are well developed. In addition, high background concentrations of individual elements spatially coincided with known tungsten polymetallic deposits.

4.4. Identification of tungsten polymetallic geochemical anomaly

Two hundred concentration realizations of individual elements were generated by means of SIS. Each of these realizations was processed further by a complied SIRs batch algorithm to generate a corresponding SIR. As a result, 200 SIRs were obtained. The variations among the SIRs provide a measure of geochemical anomaly uncertainty for targeting tungsten polymetallic mineralization and exhibit similar spatial distribution patterns across the study area. Fig. 10 shows the spatial distributions of the four SIRs that were generated from the four corresponding concentration realizations (#149) shown in Fig. 8. It can be seen that a single SIR does not clearly express continuous distribution pattern for the singularity indices due to the influence of local high and low α-values. However, the results show that the E-type α map of individual elements (W, Sn, Mo and Bi) exhibits more continuous spatial distribution pattern compared to a single SIR (Fig. 11). The results also indicate that the degree of element enrichment is inversely proportional to the singularity indices (Cheng, 2007).

Geochemical anomaly patterns characterized by smaller α-values indicate much greater spatial correlation with known tungsten polymetallic deposits (Fig. 11a, b, c, d). These patterns are mainly present at or near the Caledonian, Indosinian and Yanshanian granites and are partly located in the Devonian-Triassic sedimentary cover, which are considered to be genetically associated with tungsten polymetallic mineralization in the study area (Hua et al., 2005; Chi et al., 2012). Comparison of the distributions of original concentration data for W, Sn, Mo and Bi (Fig. 8a, b, c, and d) with those Fig. 11a, b, c and d, respectively, indicates that zones with high anomaly are further localized whereas zones with weak anomaly were enhanced greatly as depicted by singularity indices with $\alpha < 2$. For example, the weak W anomalous zones based on the original geochemical data in Fig. 8a are highlighted in the northeast parts of the study area in Fig. 11a.

4.5. Uncertainty assessment of tungsten polymetallic geochemical anomaly

Assessment of uncertainty of estimates for a target attribute involves creating a probability map of (not) exceeding a certain threshold (Goovaerts, 1997). In this paper, the S-Q method was adopted to

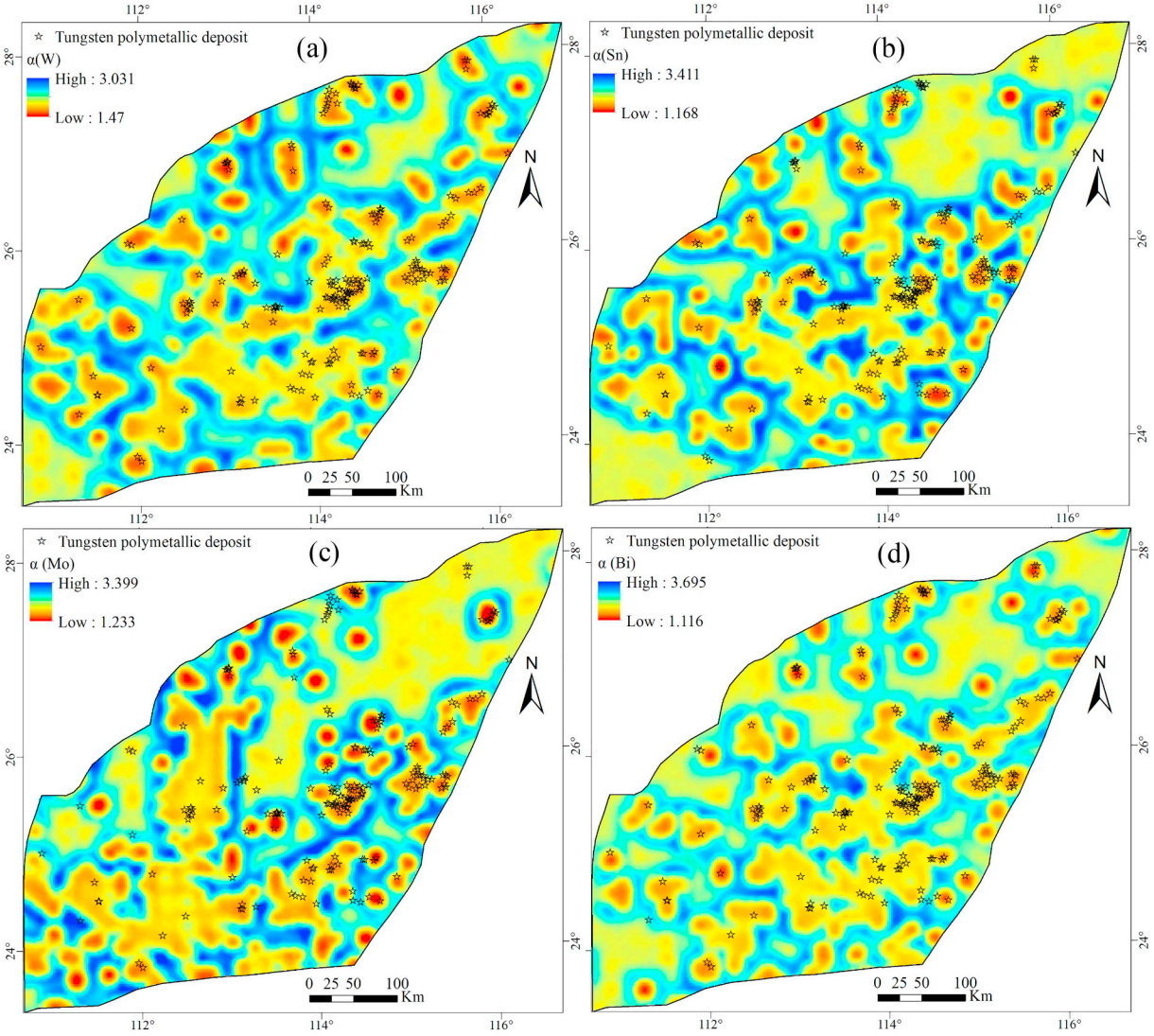

Fig. 11. Maps of the E-type α-values of elements: (a) W, (b) Sn, (c) Bi and (d) Mo.

determine geochemical anomaly thresholds based on inherent fractal/multifractal properties (Liu et al., 2017). A frequency domain plot of standard normal quantiles (x-axis) versus quantiles of E-type singularity indices (y-axis) was used to distinguish distribution patterns of E-type α-values of individual elements (W, Sn, Mo, and Bi) (Fig. 12). We set a 99% confidence interval of E-type α-values and chose a suitable percentile interval within the 15th to 85th percentile range to set the normal reference line and residual fitting curves as indicated by the red lines and blue lines, respectively, in Fig. 12a, b, c, d. Another polynomial curve with green colour was produced by fitting all the α-values (Fig. 12). Based on the two residual fitting curves and the polynomial curve, two thresholds (α_1 and α_2) of E-type α-values of each element were determined (Fig. 12a, b, c, d), showing that normal distributed E-type α-values plot near or close to the normal reference line. However, the α-values depicted by lower-truncated tail distribution plot below the fitting normal reference lines, following fractal/multifractal distribution (Liu et al., 2018b). The S-Q method provides for estimation of critical thresholds for separating E-type α-values into three different populations that may correspond to unusual physicochemical attributes caused by drastically changing geological phenomena such as lithostratigraphic contact, local mineralization, weathering product and mineral alteration phase. In practice, these critical thresholds are of great significance for geochemical anomaly separation and mapping (Liu et al., 2017).

Based on the threshold of low singularity index, such as $\alpha_W = 1.945$ (Fig. 12a), the SIRs were used to model geochemical anomaly uncertainty for targeting tungsten polymetallic mineralization by generating a probability map of not exceeding this threshold (Fig. 13a). The other three probability maps (Fig. 13b, c, and d) were obtained based on the thresholds of $\alpha_{Sn} = 1.911$, $\alpha_{Mo} = 1.946$ and $\alpha_{Bi} = 1.932$, respectively (Fig. 12b, c, and d). According to Fig. 13a, b, c, and d, the zones with little uncertainty are those related to very high probability for the occurrence of geochemical anomaly, implying that the risk for finding tungsten polymetallic deposits is very low, such as the zones indicated by red. The zones with large uncertainty are those related to very low probability for the occurrence of geochemical anomaly, implying that the risk for finding tungsten polymetallic deposits is very high, such as the zones indicated by the blue colour. In contrast, a medium probability for the occurrence of geochemical anomaly indicates moderate uncertainty, implying moderate risk for finding tungsten polymetallic deposits, such as the zones indicated by yellow and green.

Fig. 13a, b, c, d shows the probability maps of individual elements but they do not provide comprehensive and straightforward

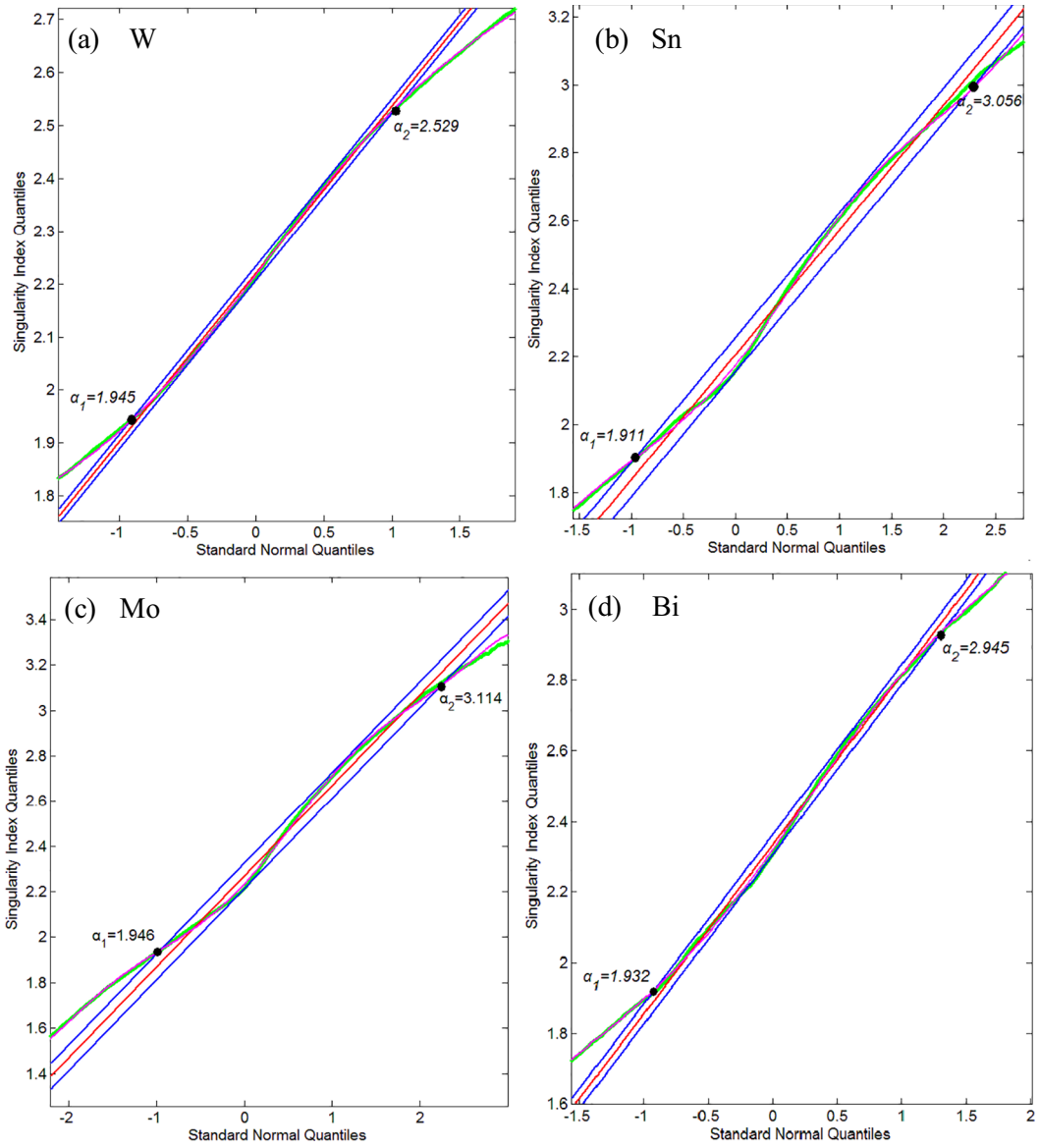

Fig. 12. Singularity index quantiles versus standard normal quantiles of (a) W, (b) Sn, (c) Mo, (d) Bi.

information for risk assessment for tungsten polymetallic exploration targeting. Therefore, a synthetic probability map was produced by integrating the four probability maps of W, Sn, Mo, and Bi into a single one (i.e., by adding the maps and taking the average per location). Fig. 14a shows this synthetic probability map overlaid with the known tungsten polymetallic deposits, indicating that there is significant correlation between the very high probability values and tungsten polymetallic deposits. Fig. 14b shows the synthetic probability map overlaid lithostratigraphic contacts. Previous studies indicate that lithostratigraphic contact is one of the most important controls on the formation of tungsten polymetallic deposit (Liu et al., 2014b, 2018d). According to Peng et al. (2006) and Liu et al. (2014b), tungsten polymetallic mineralization commonly formed at the contacts between strata and granites with significant differences in physical–chemical properties. It can be observed that the high probability zones are frequently located near lithostratigraphic contacts (Fig. 14b), implying that granites intruding the sedimentary strata are the favorable places for tungsten polymetallic mineralization, where uncertainty of tungsten polymetallic exploration targeting is very low. During the emplacement of granites, interactive geochemical reactions facilitated the occurrence of metal mineralization between country rocks due to passage of hydrothermal fluids along the lithostratigraphic contacts, which is conductive to the enrichment of metal elements (Pei et al., 2009; Wang et al., 2015). Therefore, the zones with high probability of the presence tungsten polymetallic geochemical anomaly and lithostratigraphic contacts are favorable for finding tungsten polymetallic deposits with low uncertainty. It can also be seen that very high probabilities of the presence of tungsten polymetallic geochemical anomaly are well spatially coincident with small Indosinian granite intrusions in the northern parts of the study area. Likewise, very high probabilities of the presence of tungsten polymetallic geochemical anomaly are well spatially coincident with Yanshanian granite intrusions in the southern and central parts of the study area. In contrast, very high probabilities of the presence of tungsten polymetallic geochemical anomaly are not strongly spatially coincident with Caledonian granite intrusions across the study area. Xu et al. (1982) believed that Caledonian granite intrusions in south China had nothing to do with the formation of tungsten, tin and rare metal deposits. However, recently studies indicate

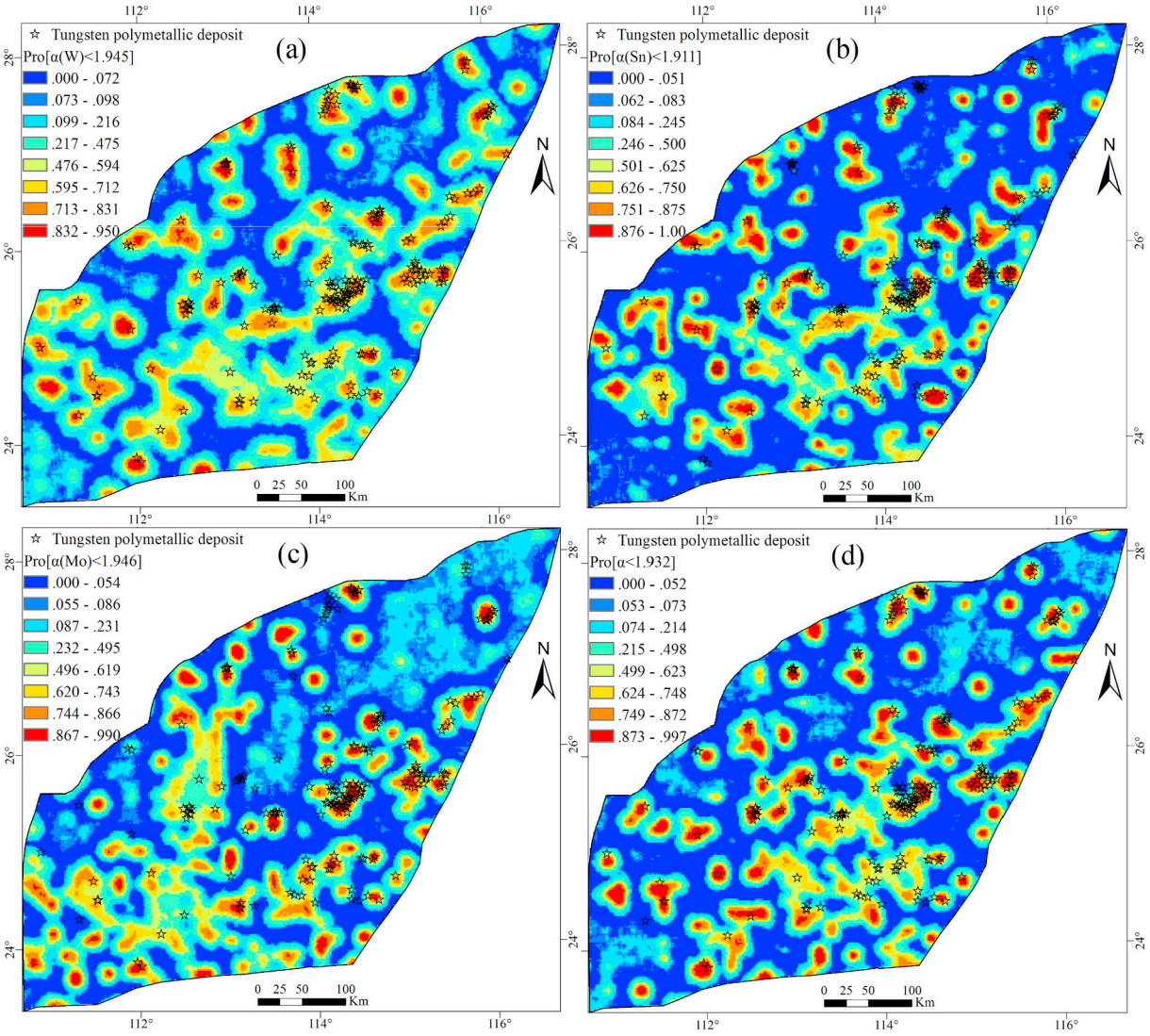

Fig. 13. Probability distribution of α-values under the condition of (a) $\alpha_W < 1.945$, (b) $\alpha_{Sn} < 1.911$, (c) $\alpha_{Mo} < 1.946$ and (d) $\alpha_{Bi} < 1.932$.

that some parts of the Caledonian granites are associated with tungsten mineralization (Zhang et al., 2011; Chen et al., 2014; Yang et al., 2014).

High probability values imply high possibility of the presence of the tungsten polymetallic deposits indicated by Fig. 14. In order to examine the performance of the synthetic probability map, first, the prediction-area (P-A) plot analysis (Yousefi and Carranza, 2015) was used to determine reasonable threshold. Then, favorable exploration targets were demarcated from the synthetic probability map based on the threshold. As shown in the Fig. 15a, the intersection point shown in Fig. 15a indicates that 18.5% of the study area can be predicted as prospective, in which 81.5% of the known deposits are contained. High favorability zones reflect strong spatial coincidence with known tungsten polymetallic deposits (Fig. 15b).

5. Conclusions

1) Quantification of geochemical anomaly uncertainty is crucial for risk assessment in exploration geochemistry. In this study, we presented a method based on combining singularity analysis and sequential indicator simulation to assist in the modelling of spatial variability and quantification of uncertainty associated with geochemical anomaly mapping for tungsten polymetallic exploration targeting in the Nanling belt, South China. The integrated method overcomes the smoothing effect of point-data interpolation and thus ensures that extreme values of geochemical data (here for W, Sn, Mo and Bi) are not eliminated, making them significantly favorable for geochemical anomaly recognition.
2) A series of equally probable realizations of element concentrations were further processed by using a compiled SIR singularity analysis. The results allow for assessing geochemical anomaly uncertainty for tungsten polymetallic exploration targeting. Thresholds of anomalous singularity indices for the selected elements were determined by the S-Q method, which is proposed, because it considers the inherent multifractal property of element distribution patterns in the Earth's Crust, and thus the post-processing SIRs are more reliable for characterizing geochemical anomaly.
3) The probabilistic models of the SIRs of the four elements W, Sn, Mo and Bi were obtained for not exceeding a threshold singularity index

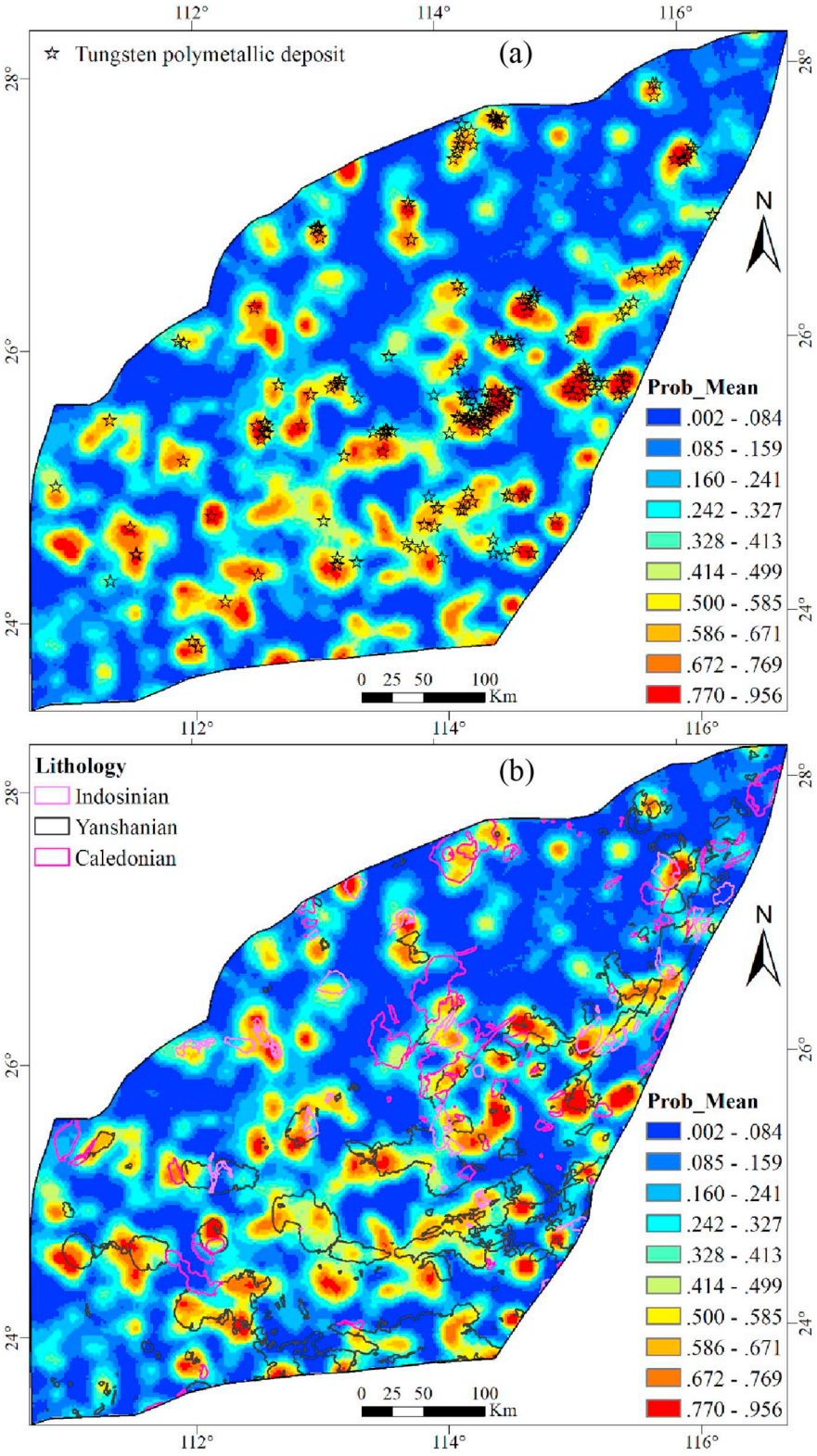

Fig. 14. Synthetic probability map calculated from average probability based on the probability of $\alpha_W < 1.945$, $\alpha_{Sn} < 1.911$, $\alpha_{Mo} < 1.946$ and $\alpha_{Bi} < 1.932$, superimposed by (a) tungsten polymetallic deposits (stars) and (b) granites (polylines with colors).

per element. According to the synthetic probability map, high probability zones are commonly coincident with lithostratigraphic contacts and have significant correlation with the known deposits. Therefore, the resulting map would be invaluable for decision-making, especially for mineral exploration risk assessment, such as determining zones that are more favorable for exploration of tungsten polymetallic mineralization.

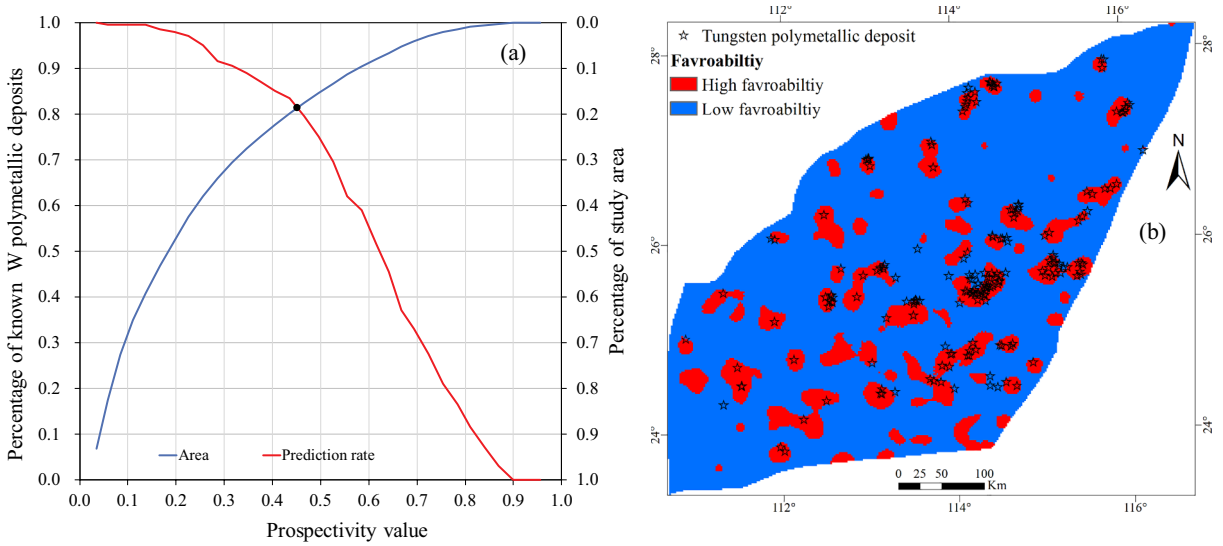

Fig. 15. (a) Prediction-area (P-A) curves for the synthetic probability map based on arithmetic mean function, (b) Binary map showing high and low favorable zones based on the P-A plot analysis.

Acknowledgements

This work was funded jointly by the National Natural Science Foundation of China (Nos. 41672328, 41702356), the project of China Postdoctoral Science Foundation (Nos. 2016M590992, 2018T111122).

References

Afzal, P., Madani, N., Shahbeik, S., Yasrebi, A.B., 2015. Multi-Gaussian kriging: a practice to enhance delineation of mineralized zones by concentration-volume fractal model in Dardevey iron ore deposit, SE Iran. J. Geochem. Explor. 158, 10–21.

Agterberg, F., 2014. Geomathematics: Theoretical Foundations, Applications and Future Developments. 18 Springer.

Cambardella, C.A., Moorman, T.B., Parkin, T.B., Karlen, D.L., Novak, J.M., Turco, R.F., Konopka, A.E., 1994. Field-scale variability of soil properties in central Iowa soils. Soil Sci. Soc. Am. J. 58 (5), 1501–1511.

Carranza, E.J.M., 2017a. Natural resources research publications on geochemical anomaly and mineral potential mapping, and introduction to the special issue of papers in these fields. Nat. Resour. Res. 26 (4), 379–410.

Carranza, E.J.M., 2017b. Geochemical mineral exploration: should we use enrichment factors or log-ratios? Nat. Resour. Res. 26 (4), 411–428.

Chen, G., Cheng, Q., 2016. Singularity analysis based on wavelet transform of fractal measures for identifying geochemical anomaly in mineral exploration. Comput. Geosci. 87, 56–66.

Chen, G., Cheng, Q., 2017. Fractal density modeling of crustal heterogeneity from the KTB deep hole. J. Geophys. Res. Solid Earth 122 (3), 1919–1933.

Chen, Y., Wu, W., 2017. Application of one-class support vector machine to quickly identify multivariate anomalies from geochemical exploration data. Geochem.: Explor., Environ., Anal. 17 (3), 231–238.

Chen, Y., Pei, R., Zhang, H., Lin, X., Bai, G., Li, C., Hu, Y., Liu, G., Xian, B., 1989. The Geology of Non-ferrous and Rare Metal Deposits Related to Mesozoic Granitoids in Nanling Region. Geological Publishing House, Beijing (in Chinese).

Chen, J., Lu, J., Chen, W., Wang, R.C., Ma, D., Zhu, J., Zhang, W., Ji, J., 2008. W–Sn–Nb–Ta-bearing granites in the Nanling range and their relationship to metallogengesis. J. China Univ. Geosci. 14, 459–473 (in Chinese with English abstract).

Chen, J., Wang, R., Zhu, J., Lu, J., Ma, D., 2013. Multiple-aged granitoids and related tungsten-tin mineralization in the Nanling Range, South China. Sci. China Earth Sci. 56 (12), 2045–2055.

Chen, J., Wang, R., Zhu, J., Lu, J., Ma, S., 2014. Multiple-aged granitoids and related tungsten-tin mineralization in the Nanling Range, South China. Sci. China Earth Sci. 56 (1), 111–121 (in Chinese with English abstract).

Chen, G., Cheng, Q., Zuo, R., Liu, T., Xi, Y., 2015. Identifying gravity anomalies caused by granitic intrusions in Nanling mineral district, China: a multifractal perspective. Geophys. Prospect. 63, 256–270.

Cheng, Q., 2007. Mapping singularities with stream sediment geochemical data for prediction of undiscovered mineral deposits in Gejiu, Yunnan Province, China. Ore Geol. Rev. 32 (1), 314–324.

Cheng, Q., 2016. Fractal density and singularity analysis of heat flow over ocean ridges. Sci. Rep. 6, 19167.

Cheng, Q., Agterberg, F.P., 2009. Singularity analysis of ore-mineral and toxic trace elements in stream sediments. Comput. Geosci. 35 (2), 234–244.

Cheng, Q., Agterberg, F., 2018. Preface: multifractals and singularity analysis in mineral exploration and environmental assessment. J. Geochem. Explor. 189, 1.

Chi, Q., Wang, X., Xu, F., Zhou, J., Liu, H., Liu, D., Zhang, B., Wang, W., 2012. Temporal and spatial distribution of tungsten and tin in South China Continent. Earth Sci. Front. 19 (3), 70–83 (in Chinese with English abstract).

Cracknell, M.J., de Caritat, P., 2017. Catchment-based gold prospectivity analysis combining geochemical, geophysical and geological data across northern Australia. Geochem.: Explor., Environ., Anal. 17 (3), 204–216.

de Souza, L.E., Costa, J.F.C., 2013. Sample weighted variograms on the sequential indicator simulation of coal deposits. Int. J. Coal Geol. 112, 154–163.

Deutsch, C.V., 2006. A sequential indicator simulation program for categorical variables with point and block data: BlockSIS. Comput. Geosci. 32 (10), 1669–1681.

Deutsch, C.V., Journel, A.G., 1998. Geostatistical Software Library and User's Guide. Oxford University Press, New York.

Emery, X., 2004. Properties and limitations of sequential indicator simulation. Stoch. Env. Res. Risk A. 18 (6), 414–424.

Emery, X., Ortiz, J.M., 2012. Enhanced coregionalization analysis for simulating vector Gaussian random fields. Comput. Geosci. 42, 126–135.

Goovaerts, P., 1997. Geostatistics for Natural Resources Evaluation. Oxford University Press, New York.

Goovaerts, P., 2001. Geostatistical modelling of uncertainty in soil science. Geoderma 103 (1–2), 3–26.

Hosseini, S.A., Asghari, O., 2018. Multivariate geostatistical simulation on block-support in the presence of complex multivariate relationships: iron ore deposit case study. Nat. Resour. Res. https://doi.org/10.1007/s11053-018-9379-2.

Hu, R., Zhou, M., 2012. Multiple Mesozoic mineralization events in South China—an introduction to the thematic issue. Mineral. Deposita 47 (6), 579–588.

Hu, R., Fu, S., Huang, Y., Zhou, M.F., Fu, S., Zhao, C., Xiao, J., 2017. The giant South China Mesozoic low-temperature metallogenic domain: reviews and a new geodynamic model. J. Asian Earth Sci. 137, 9–34.

Hua, R., Chen, P., Zhang, W., Yao, J., Lin, J., Zhang, Z., Gu, S., 2005. Metallogeneses and their geodynamic settings related to Mesozoic granitoids in the Nanling range. Geol. J. China Univ. 11 (3), 291–304 (in Chinese with English Abstract).

Hua, R., Zhang, W., Li, G., Hu, D., Wang, X., 2008. A preliminary study on the features and geologic implication of the accompanying metal in tungsten deposits in the Nanling Region. Geol. J. China Univ. 14 (4), 527–538 (in Chinese with English Abstract).

Juang, K., Chen, Y., Lee, D., 2004. Using sequential indicator simulation to assess the uncertainty of delineating heavy-metal contaminated soils. Environ. Pollut. 127 (2), 229–238.

Li, Y., 1991. Mineralogy of Tungsten Deposits in Nanling and Neighboring Area, China. China University of Geosciences Press, pp. 455 (in Chinese).

Li, Y., Zhao, W., Zhou, M., 2017. Nature of parent rocks, mineralization styles and ore genesis of regolith-hosted REE deposits in South China: an integrated genetic model. J. Asian Earth Sci. 148, 65–95.

Liu, Y., Cheng, Q., Xia, Q., Wang, X., 2013. Application of singularity analysis for mineral potential identification using geochemical data—a case study: nanling W–Sn–Mo polymetallic metallogenic belt, South China. J. Geochem. Explor. 134, 61–72.

Liu, Y., Cheng, Q., Xia, Q., Wang, X., 2014a. Identification of REE mineralization-related geochemical anomalies using fractal/multifractal methods in the Nanling belt, South China. Environ. Earth Sci. 72 (12), 5159–5169.

Liu, Y., Cheng, Q., Xia, Q., Wang, X., 2014b. Mineral potential mapping for tungsten polymetallic deposits in the Nanling metallogenic belt, South China. J. Earth Sci. 25 (4), 689–700.

Liu, Y., Cheng, Q., Zhou, K., Xia, Q., Wang, X., 2016. Multivariate analysis for

geochemical process identification using stream sediment geochemical data: a perspective from compositional data. Geochem. J. 50 (4), 293–314.
Liu, Y., Zhou, K., Cheng, Q., 2017. A new method for geochemical anomaly separation based on the distribution patterns of singularity indices. Comput. Geosci. 105, 139–147.
Liu, Y., Cheng, Q., Carranza, E.J.M., Zhou, K., 2018a. Assessment of geochemical anomaly uncertainty through geostatistical simulation and singularity analysis. Nat. Resour. Res. https://doi.org/10.1007/s11053-018-9388-1.
Liu, Y., Cheng, Q., Zhou, K., 2018b. New insights into element distribution patterns in geochemistry: a perspective from fractal density. Nat. Resour. Res. https://doi.org/10.1007/s11053-018-9374-7.
Liu, Y., Zhou, K., Carranza, E.J.M., 2018c. Compositional balance analysis for geochemical pattern recognition and anomaly mapping in the western Junggar region, China. Geochem.: Explor., Environ., Anal. 18, 263–276.
Liu, Y., Zhou, K., Xia, Q., 2018d. A MaxEnt model for mineral prospectivity mapping. Nat. Resour. Res. 27 (3), 299–313.
Mao, J., Xie, G., Guo, C., Chen, Y., 2007. Large-scale tungsten-tin mineralization in the Nanling region South China: metallogenic ages and corresponding geodynamic processes. Acta Petrol. Sin. 23 (10), 2329–2338 (in Chinese with English Abstract).
Mao, J., Cheng, Y., Chen, M., Pirajno, F., 2013. Major types and time-space distribution of Mesozoic ore deposits in South China and their geodynamic settings. Mineral. Deposita 48 (3), 267–294.
Mery, N., Emery, X., Cáceres, A., Ribeiro, D., Cunha, E., 2017. Geostatistical modeling of the geological uncertainty in an iron ore deposit. Ore Geol. Rev. 88, 336–351.
Paithankar, A., Chatterjee, S., 2018. Grade and tonnage uncertainty analysis of an African copper deposit using multiple-point geostatistics and sequential gaussian simulation. Nat. Resour. Res. 27 (4), 419–436.
Parsa, M., Maghsoudi, A., Carranza, E.J.M., Yousefi, M., 2017. Enhancement and mapping of weak multivariate stream sediment geochemical anomalies in Ahar Area, NW Iran. Nat. Resour. Res. 26 (4), 443–455.
Pei, R., Wang, Y., Wang, H., 2009. Ore-forming specialty of the tectono-magmatic zone in Nanling region and its emplacement dynamics for metallogenic series of W-Sn polymetallic deposits. Geol. China 36 (3), 483–489 (in Chinese with English Abstract).
Peng, J., Zhou, M., Hu, R., Shen, N., Yuan, S., Bi, X., Du, A., Qu, W., 2006. Precise molybdenite Re-Os and mica Ar-Ar dating of the Mesozoic Yaogangxian tungsten deposit, central Nanling district, South China. Mineral. Deposita 41, 661–669.
Qu, J., Deutsch, C.V., 2018. Geostatistical simulation with a trend using Gaussian mixture models. Nat. Resour. Res. 27 (3), 347–363.
Qu, M., Huang, B., Li, W., Zhang, C., Zhao, Y., 2015. Spatial uncertainty of joint health risk of multiple trace metals in rice grain in Jiaxing city, China. Environ. Sci.: Processes Impacts 17 (1), 120–130.
Rahimi, H., Asghari, O., Hajizadeh, F., 2018. Selection of optimal thresholds for estimation and simulation based on indicator values of highly skewed distributions of ore data. Nat. Resour. Res. 27 (4), 437–453.
Remy, N., Boucher, A., Wu, J., 2009. Applied Geostatistics with SGeMS: a User's Guide. Cambridge University Press, New York.
Sadeghi, B., Madani, N., Carranza, E.J.M., 2015. Combination of geostatistical simulation and fractal modeling for mineral resource classification. J. Geochem. Explor. 149, 59–73.
Shu, L., Zhou, X., Deng, P., Yu, X., 2006. Principal geological features of Nanling Tectonic Belt, South China. Geol. Rev. 52, 251–265 (in Chinese with English abstract).
Sun, T., Zhou, X., Chen, P., Li, H., Zhou, H., Wang, Z., Shen, W., 2003. Genesis and tectonic significance of Mesozoic strong peraluminous granites in Eastern Nanling region. Sci. China Ser. D Earth Sci. 33, 1209–1218.
Tan, Q., Wang, X., Xia, Y., Liu, Q., Zhou, J., 2018. Identifying ore-related anomalies using singularity mapping of stream sediment geochemical data, a case study of Pb mineralization in the Qinling region, China. Geochem.: Explor., Environ., Anal. 18, 177–184.
Wang, X., Zhang, Q., Zhou, G., 2007. National-scale geochemical mapping projects in China. Geostand. Geoanal. Res. 31 (4), 311–320.
Wang, X., Ni, P., Yuan, S., Wu, S., 2012. Fluid inclusion studies of the Huangsha quartz-vein type tungsten deposit, Jiangxi province. Acta Petrol. Sin. 28, 122–132 (in Chinese with English abstract).
Wang, Y., Fan, W., Zhang, G., Zhang, Y., 2013. Phanerozoic tectonics of the South China Block: key observations and controversies. Gondwana Res. 23 (4), 1273–1305.
Wang, W., Zhao, J., Cheng, Q., Carranza, E.J.M., 2015. GIS-based mineral potential modeling by advanced spatial analytical methods in the southeastern Yunnan mineral district, China. Ore Geol. Rev. 71, 735–748.
Wang, W., Cheng, Q., Tang, J., Song, Y., Li, Y., Liu, Z., 2017. Fractal/multifractal analysis in support of mineral exploration in the Duolong mineral district, Tibet, China. Geochem.: Explor., Environ., Anal. 17 (3), 261–276.
Wei, S., Jia, B., Zeng, Q., 2006. Metallogenic mechanism of tungsten deposit in Nanling area. Resour. Surv. Environ. 27 (2), 103–109 (in Chinese with English abstract).
Xiao, F., Chen, J., Hou, W., Wang, Z., Zhou, Y., Erten, O., 2018. A spatially weighted singularity mapping method applied to identify epithermal Ag and Pb-Zn polymetallic mineralization associated geochemical anomaly in Northwest Zhejiang, China. J. Geochem. Explor. 189, 122–137.
Xie, X., Mu, X., Ren, T., 1997. Geological mapping in China. J. Geochem. Explor. 60, 99–113.
Xu, K., Zhu, J., 1988. Time and space distribution of tin/tungsten deposits in South China and controlling factors of mineralization. In: Hutchison, C.S. (Ed.), Geology of Tin Deposits in Asia and the Pacific. Springer-Verlag, New York, pp. 265–277.
Xu, K., Sun, N., Wang, D., Hu, S., Liu, Y., Ji, S., 1982. On the origin and metallogeny of the granites in South China. In: Geology of Granites and their Metallogenetic Relations. Proceeding of International Symposium, Nanjing University Science Press, Beijing, pp. 1–3.
Xu, X., O'Reilly, S.Y., Griffin, W.L., Deng, P., Pearson, N.J., 2005. Relict Proterozoic basement in the Nanling Mountains (SE China) and its tectonothermal overprinting. Tectonics 24, TC2003.
Yang, Z., Wang, R., Zhang, W., Chu, Z., Chen, J., Zhu, J., Zhang, R., 2014. Skarn-type tungsten mineralization associated with the Caledonian (Silurian) Niutangjie granite, northern Guangxi, China. Sci. China Earth Sci. 44 (7), 1551–1566 (in Chinese with English abstract).
Yousefi, M., 2017. Recognition of an enhanced multi-element geochemical signature of porphyry copper deposits for vectoring into mineralized zones and delimiting exploration targets in Jiroft area, SE Iran. Ore Geol. Rev. 83, 200–214.
Yousefi, M., Carranza, E.J.M., 2015. Prediction-area (P-A) plot and C-A fractal analysis to classify and evaluate evidential maps for mineral prospectivity modeling. Comput. Geosci. 79, 69–81.
Yousefi, M., Carranza, E.J.M., Kamkar-Rouhani, A., 2013. Weighted drainage catchment basin mapping of geochemical anomalies using stream sediment data for mineral potential modeling. J. Geochem. Explor. 128, 88–96.
Yuan, F., Li, X., Zhou, T., Deng, Y., Zhang, D., Xu, C., Jowitt, S.M., 2015. Multifractal modelling-based mapping and identification of geochemical anomalies associated with Cu and Au mineralisation in the NW Junggar area of northern Xinjiang Province, China. J. Geochem. Explor. 154, 252–264.
Zhang, W., Wang, R., Lei, Z., Hua, R., Zhu, J., Lu, J., Xie, L., Hua, X., Zhang, R., Yao, Y., Chen, J., 2011. The found of containing scheelite Penggongmiao Caledonian aplite in southern Hunan. Chin. Sci. Bull. 56 (18), 1448–1454 (in Chinese).
Zhang, D., Cheng, Q., Agterberg, F., Chen, Z., 2016. An improved solution of local window parameters setting for local singularity analysis based on Excel VBA batch processing technology. Comput. Geosci. 88, 54–66.
Zhao, Y., Shi, X., Yu, D., Wang, H., Sun, W., 2005. Uncertainty assessment of spatial patterns of soil organic carbon density using sequential indicator simulation, a case study of Hebei province, China. Chemosphere 59 (11), 1527–1535.
Zhao, J., Wang, W., Dong, L., Yang, W., Cheng, Q., 2012. Application of geochemical anomaly identification methods in mapping of intermediate and felsic igneous rocks in eastern Tianshan, China. J. Geochem. Explor. 122, 81–89.
Zhao, W., Zhou, M., Li, Y., Zhao, Z., Gao, J., 2017. Genetic types, mineralization styles, and geodynamic settings of Mesozoic tungsten deposits in South China. J. Asian Earth Sci. 137, 109–140.
Zhou, X., 2003. My thinking about granite geneses of South China. Geol. J. China Univ. 9, 556–565 (in Chinese with English abstract).
Zhou, X., Sun, T., Shen, W., Shu, L., Niu, Y., 2006. Petrogenesis of Mesozoic granitoids and volcanic rocks in South China: a response to tectonic evolution. Episodes 29, 26–33.
Zuo, R., 2017. Machine learning of mineralization-related geochemical anomalies: a review of potential methods. Nat. Resour. Res. 26 (4), 457–464.